Engineering 5 (2019) 329–336

Contents lists available at ScienceDirect

Engineering

journal homepage: www.elsevier.com/locate/eng

Research
Rail Transit—Article

Numerical and Experimental Study on Ventilation Panel Models in a Subway Passenger Compartment

Yu Tao [a], Mingzhi Yang [a,b], Bosen Qian [a,b], Fan Wu [a,b], Tiantian Wang [a,b,*]

[a] Key Laboratory of Traffic Safety on Track, Ministry of Education, School of Traffic and Transportation Engineering, Central South University, Changsha 410075, China
[b] Joint International Research Laboratory of Key Technologies for Rail Traffic Safety, Changsha 410075, China

ARTICLE INFO

Article history:
Received 11 October 2018
Revised 27 November 2018
Accepted 29 December 2018
Available online 2 March 2019

Keywords:
Numerical simulation
Experiment
Ventilation panel model
Subway

ABSTRACT

The internal flow field study of car compartments is an important step in railroad vehicle design and optimization. The flow field profile has a significant impact on the temperature distribution and passenger comfort level. Experimental studies on flow field can yield accurate results but carry a high time and computational cost. In contrast, the numerical simulation method can yield an internal flow field profile in less time than an experimental study. This study aims to improve the computational efficiency of numerical simulation by adapting two simplified models—the porous media model and the porous jump face model—to study the internal flow field of a railroad car compartment. The results provided by both simplified models are compared with the original numerical simulation model and with experimental data. Based on the results, the porous media model has a better agreement with the original model and with the experimental results. The flow field parameters (temperature and velocity) of the porous media model have relatively small numerical errors, with a maximum numerical error of 4.7%. The difference between the numerical results of the original model and those of the porous media model is less than 1%. By replacing the original numerical simulation model with the porous media model, the flow field of subway car compartments can be calculated with a reduction of about 25% in computing resources, while maintaining good accuracy.

1. Introduction

During subway operation, the air temperature inside subway compartments should be kept within a specified range. This climate-control process is realized through a heating, ventilation, and air conditioning (HVAC) system, through which air is exchanged across the boundaries of the chamber via mechanical ventilation [1]. Existing studies on the performance of an HVAC system in a closed chamber have mainly focused on buildings, airplanes, and vehicles. A steady airflow field was first simulated, and was then compared with experimental data [1]. Dehghan and Abdolzadeh [2], Zhuang et al. [3], and Pang et al. [4] simulated the air flow in a room and in a civil aircraft cabin using a three-dimensional (3D) model with a thermal manikin. The fluid flow was simulated by the steady Reynolds-averaged Navier–Stokes (RANS) equations with a v^2-f turbulence model and the re-normalization group (RNG) k-ε turbulence model, respectively. As the air-flow and temperature fields inside the cabin are in fact unsteady, the unsteady RANS (URANS) equation is used for internal flow simulation. The standard k-ε turbulence model [5,6] and the RNG k-ε turbulence model [7,8] are widely used for simulating the turbulent flow field inside a chamber.

Existing studies on railroad vehicle HVAC systems have mainly focused on the HVAC system parameters and vehicle structures. Dullinger et al. [9] invented a simulation approach that combines the HVAC system with a dynamic thermal vehicle model and includes operational and weather inputs. Hofstädter et al. [10] and Luger et al. [11] studied dynamic thermal models of railroad vehicles and the operating conditions of HVAC systems. Their results show that the parameters of the HVAC system and the vehicle structures strongly influence the thermal comfort and air-supply uniformity in subway passenger compartments. Schmeling and Bosbach [12] and Li and Sun [13] investigated the dynamic cooling load and ventilation efficiency of metro and railway cars through numerical simulation. They concluded that the cooling performance is limited by the rate of fresh air available through the fresh air. Liu et al. [14] discussed the effects of ambient

* Corresponding author.
E-mail address: wangtiantian@csu.edu.cn (T. Wang).

https://doi.org/10.1016/j.eng.2018.12.007

conditions and human thermal emission based on different cooling loads, and provided a solid basis for the determination of cooling load for trains traveling in different regions and over various periods of time. Suárez et al. [15] investigated the air distribution in a representative railway vehicle equipped with an HVAC system. The heat transfer of the wall and the heat load of passengers were both considered in their study. Wang et al. [16] investigated the performance evaluation of air-distribution systems in three different China railway high-speed train cabins using numerical simulation. Aliahmadipour et al. [17] proposed compartment modifications for passenger coaches, which can lead to better thermal conditions for the passengers seated or sleeping in the compartment.

Ventilation panels are commonly installed at the air inlet of a passenger compartment for better flow uniformity. Each ventilation panel is composed of a block with a large number of small ventilation holes assembled in a matrix form. In a numerical simulation, these small ventilation holes require a small-scale mesh treatment. Thus, the small elements near the ventilation panel will significantly increase the computational cost. In this study, two simplified models are proposed to improve the numerical simulation efficiency. The results given by the simplified models are then validated by a full-scale (original) simulation model as well as by experimental measurement results. One of the simplified models can reduce the computation time in a numerical simulation with a minor compromise in terms of the accuracy of the results. The model proposed in this work can serve as a convenient tool in future studies on internal flow fields and temperature profiles of subway passenger compartments.

2. Numerical simulation

2.1. Geometric model

A specific type of subway middle car was adopted for the current study that includes a passenger compartment, two passageways, an HVAC system, and an air-duct system. Fig. 1 provides a geometric model of the subway car. The height and width of the subway middle car are defined as H and W, respectively. L_1 is the length of passenger compartment and L_2 is the length of one passageway. The two air conditioners of the HVAC system are set at the top of the passenger compartment, and each of the air conditioners has two outlets and one inlet. For numerical simulation of the air conditioner, a method using the velocity inlet and the outlet boundary condition was adopted instead of the real model. The red-dotted boxes in Fig. 1(a) represent the position of the air conditioners. The air-duct system consists of supply, recirculated, and exhaust air ducts. Fresh air from the air conditioner outlet enters the passenger compartment through the supply air duct. Air in the passenger compartment flows to the air conditioner through the recirculated air duct, and then passes out to the atmosphere through the exhaust air duct. The green part of the figure represents the supply air duct, which is symmetrical around the central axis. The units of the supply air duct on the same side are inter-connected, and the air inlets of the passenger compartment are set at the top and side along the direction of the subway car length. The red and yellow parts of the figure represent the recirculated and exhaust air ducts, respectively. The purple part of the figure represents the seats; four groups of seats are symmetrically set around the central axis. As the seats are next to the subway car surface, they are treated as the surface boundary for the numerical simulation. For analysis, the front and back of the passenger compartment are defined as End I and End II, as shown in Fig. 1(a).

Fig. 2 shows a cross-section of the supply air duct. The duct is set on top of the passenger compartment and consists of five parts (1–5 in Fig. 2). The height of the five parts (1–5) are defined as ΔZ_1, ΔZ_2, ΔZ_3, and ΔZ_4, respectively. Part 6 represents the passenger compartment, with the typical connection faces of each part defined as A–D. Part 1 connects the air conditioner and part 2—that is, the bulge of the green part in Fig. 1. Part 1 is located at the position of the air conditioner, instead of along the whole length of the subway car. Parts 2, 3, and 5 are channels that are distributed along the entire length of the subway car. Fresh air is sent into the passenger compartment through these channels.

The inside of part 2 contains a baffle that provides air flow to both sides, and the vents on both sides are labeled as the connection face B, as shown in Fig. 3(a). Part 4 in this figure represents a square channel connecting parts 3 and 5. As can be observed in Fig. 2, parts 2 and 3 are located outside of the passenger compartment, while part 5 is located inside. Fresh air is sent into part 1 through face A; it then flows in the direction of the arrow, and is sent into the passenger compartment through upper (D_2 and D_3) and lateral (D_1 and D_4) ventilation panels.

The ventilation panel shown in Fig. 3 is used to ensure air-supply uniformity along the length of the subway car. Based on the engineering requirements, two kinds of ventilation panel are adopted for the upper and lateral sides, as shown in Figs. 3(b) and (c). The thickness of the upper ventilation panel is 2 mm, and the ventilation hole is a circle with a radius of 2.5 mm and a porosity rate of 0.087. The thickness of the lateral ventilation panel is 4 mm and the ventilation hole is 43 mm long and 7 mm wide, with a porosity rate of 0.257.

2.2. Mesh and boundary conditions

An unstructured grid was selected for the numerical simulation. The mesh density around the supply air duct and passenger compartment surface is high. The first layer of the boundary grid around the compartment surface is 3 mm. and the total grid

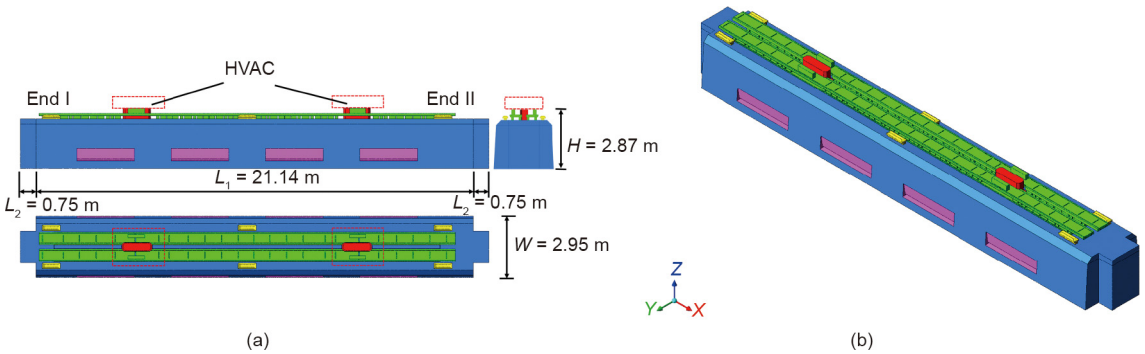

Fig. 1. A geometric model of the subway car. (a) Dimensional drawing; (b) schematic.

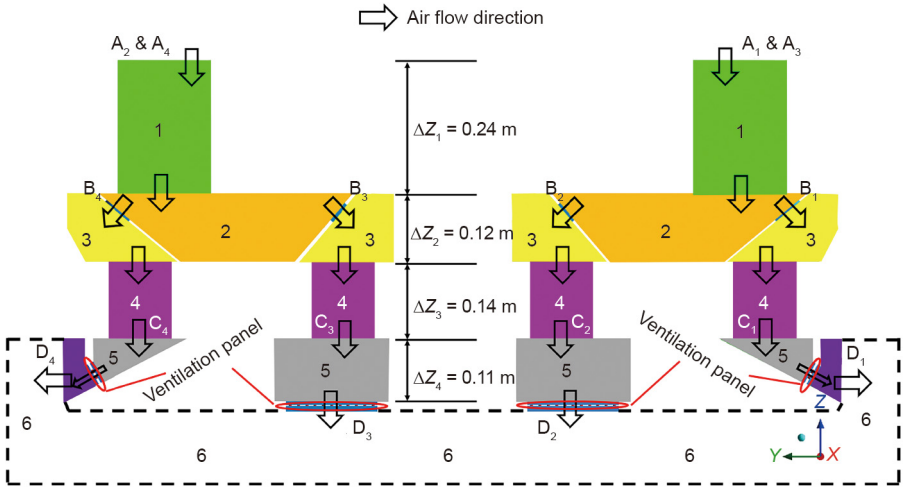

Fig. 2. A cross-section of the supply air duct.

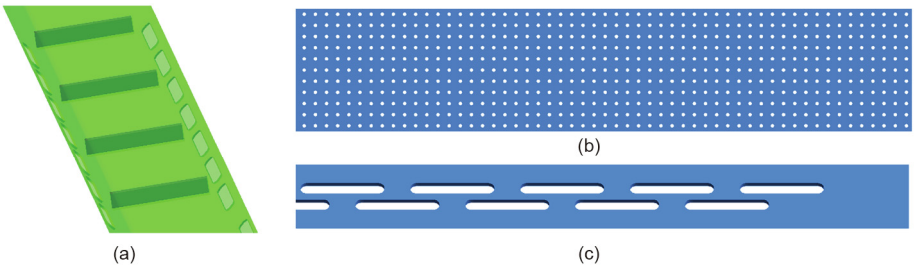

Fig. 3. The model schematic. (a) Model of part 2 in Fig. 2; (b) upper ventilation panel model; (c) lateral ventilation panel model.

number is 0.11 billion. The local surface mesh is shown in Fig. 4. The internal flow field of a subway car is turbulent. The k-ε turbulence model is commonly used to compute turbulent flow, and the y+ (the dimensionless first-cell spacing $y+ = y \cdot u_t \cdot \eta^{-1}$, where y is the thickness of the first-cell near the wall, u_t is the friction velocity and η is the kinetic viscosity) range for turbulence models in this process must be 30–100. The average y+ of the mesh constructed in this simulation is about 33, and thus meets the range requirements. In order to ensure that the mesh has no effect on the numerical calculation results when using the porous media model and the porous jump surface model (described in Section 3), only the grid of the ventilation panel area is changed; the grids of the other regions remain unchanged. Thus, the mesh of the two models satisfy the requirement of y+ value.

The boundary conditions set in this manuscript are as follows:

(1) The air conditioner outlet, recirculated air-duct inlet, and exhaust air-duct inlet are set as the mass flow inlet boundary conditions. When the value of the mass flow is negative, air flows outside of the computational domain. The flow rates of supply, recirculated, and exhaust air are 10 000 $m^3 \cdot h^{-1}$, −6800 $m^3 \cdot h^{-1}$, and −3200 $m^3 \cdot h^{-1}$, respectively. According to the area of the corresponding inlets and outlets, the velocities of supply, recirculated, and exhaust air are 5.261 $m \cdot s^{-1}$, −1.937 $m \cdot s^{-1}$, and −3.922 $m \cdot s^{-1}$, respectively.

(2) The passenger compartment surface is set as the heat-flux wall boundary condition, with a heat-transfer coefficient of 2.5 $W \cdot (m^2 \cdot K)^{-1}$, defined as the K value. A definition for "K value" can be found in Ref. [18].

(3) All surfaces are set as no-slip wall boundary conditions.

(4) This study examines full-passenger working conditions in summer. That is to say, it is assumed that there are 310 passengers in the compartment. And the outside temperature is set at a constant 33 °C. Due to the considerable amount of thermal energy produced by a human, human heat sources are considered in the numerical simulation. The human heat sources are set as 120 W per person, according to the European standard EN14750 [19],

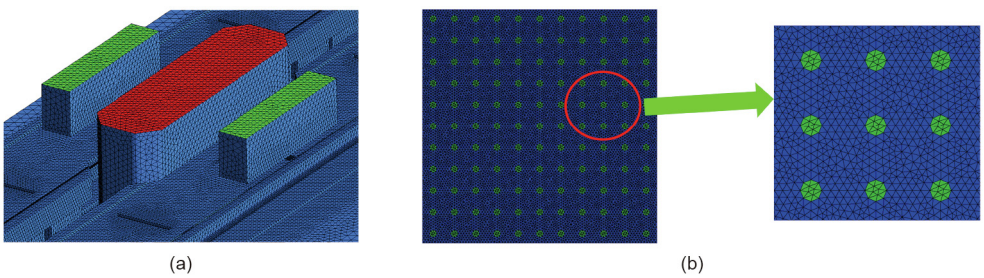

Fig. 4. The local surface mesh. (a) Air conditioner; (b) upper ventilation panel.

and are loaded as volumetric sources into the corresponding human-activity area of the computational domain. The volumetric heat source is set as 294.5 $W \cdot m^{-3}$. As the passenger compartment contains a large number of heat sources (i.e., humans), the fresh air temperature is set at 13 °C.

(5) Three types of ventilation panel model for the numerical simulation are tested in this study: the original model, porous media model, and porous jump face model. Detailed information is provided in Section 3.

2.3. Measurement point

An experiment involving a real train compartment was also carried out in this study. The positions of the measurement points (the black and red points in Fig. 5) were set based on the European standard EN14750. The velocity and temperature of the air at each measurement point were tested. According to the standard, the average velocity and temperature at nine horizontal measurement points (points 1–9) was defined as the average velocity and temperature of the air in the passenger compartment (v_a and T_a). The maximum differences were defined as the horizontal velocity and temperature difference (v_x and T_x). The maximum differences in the velocity and temperature at nine vertical measurement points (points 2, 5, 8, and 10–15) were defined as the vertical velocity and temperature differences (v_z and T_z). The coordinate value of the position along the *X*-axis, *Y*-axis, and *Z*-axis are defined as *X*, *Y*, and *Z*, respectively.

2.4. Numerical method

In this paper, numerical simulations of the internal flow field of a subway middle car were conducted using ANSYS Fluent, which is a finite-volume-method-based solver. The URANS method and the RNG k-ε turbulence model were selected for the numerical simulation; their governing equations can be found in Refs. [20] and [21]. As the air velocity in a passenger compartment is relatively slow, the air was assumed to be incompressible. As the heat transfer of the internal flow field occurs within a closed chamber, the Boussinesq hypothesis was employed to address the thermal buoyancy flow [22–24]. The definition of this hypothesis is provided in Refs. [25] and [26].

3. Ventilation panel model

Three types of ventilation panel model were selected for numerical simulation in this study. The numerical simulation model based on the actual dimensions of the ventilation panel was defined as the "original model." As the original model requires a great deal of computational power for numerical simulation, the porous media model and porous jump face model have been widely used for numerical simulation of the internal flow field [27,28]. The present study focuses on the numerical simulation of an internal flow field using the proposed ventilation panel models.

For the porous media model, the ventilation panel is defined as a unit body. Given the porous media parameters, the pressure loss of the air flowing through the ventilation panel can be obtained, as shown in Eq. (1) [29]:

$$\Delta p = \frac{1}{2} C_2 \cdot \rho \cdot \Delta n \cdot v^2 + \frac{\mu}{\alpha} \cdot \Delta n \cdot v \tag{1}$$

where Δp represents the pressure loss (Pa); μ represents the aerodynamic viscosity, set as 1.8×10^{-5} Pa·s in this study; v represents the air velocity ($m \cdot s^{-1}$); C_2 represents the inertia resistance coefficient (m^{-1}); α represents the surface permeability (m^2); ρ represents the air density, set as 1.225 $kg \cdot m^{-3}$; and Δn represents the thickness of the ventilation panel, set as 2 and 4 mm for the upper and lateral panels, respectively.

The porous jump face model can be regarded as a one-dimensional (1D) simplification of the porous media model. The ventilation panel is defined as a unit surface, and Eq. (1) can be applied in the same way.

The pressure loss of the upper and lateral ventilation panels at different air velocities was obtained by means of experiments in this study. An experiment on ventilation panels was carried out at the Central South University model test platform in China, which has obtained China Metrology Accreditation (CMA) qualification (certificate number 2014002479K). More detailed information about the platform is provided in Refs. [30] and [31]. The air velocities were 1, 2, 3, 4, and 5 $m \cdot s^{-1}$. The experimental model was constructed according to the actual size of the ventilation panel, as shown in Fig. 6(a). A Honeywell DC030NDC4 pressure sensor was selected for pressure measurement, as shown in Fig. 6(b). The sampling frequency of the sensors was 1 kHz in this set of tests, and the measurement accuracy was 0.01 Pa. For velocity measurement, a TSI9525 anemometer with a hot-wire wind-speed probe was adopted, with a measurement accuracy of 0.01 $m \cdot s^{-1}$. Before each test, every sensor had to be recalibrated and calibrated. The error of the loading test was within 0.2%, which is considered to meet the test accuracy requirements. Each case was repeated five times, and the acceptability in terms of air velocity was examined. Tests that did not meet the required accuracy of ±0.2% of the target air velocity were discarded. The average of the data from the five tests was defined as the experimental results. Table 1 shows the experimental results for ventilation panel pressure loss. In this table, v and Δp are the same variables as in Eq. (1), and "upper" and "lateral" represent the upper and lateral ventilation panels. Table 2 provides the fitting equations and fitting goodness of the ventilation panel pressure loss based on the experimental results. In this table, R^2 represents the fitting measure cofficients. Introducing the constants into the coefficients in Table 2 yields the porous media parameters $1/\alpha$ and C_2 of the ventilation panel, as shown in Table 3.

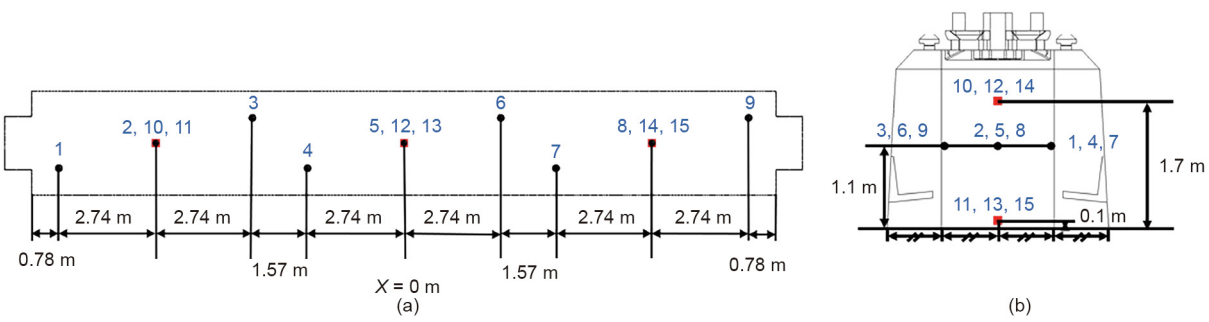

Fig. 5. A dimensional drawing of the measurement points within the real-life railway car under testing. (a) Top view; (b) front view.

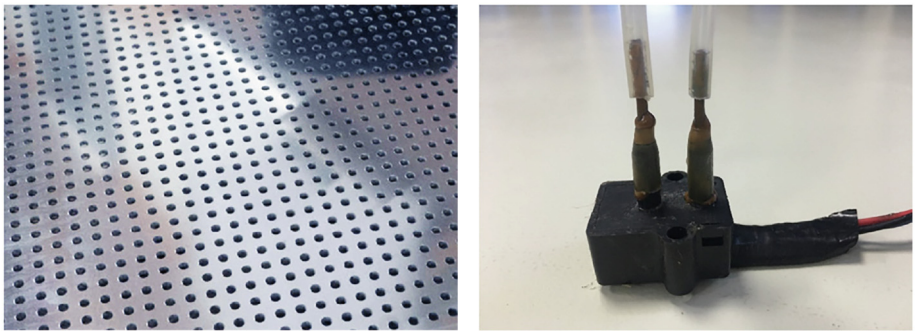

(a) (b)

Fig. 6. Experimental model and sensor. (a) Ventilation panel model; (b) pressure sensor.

Table 1
Experimental results for ventilation panel pressure loss at different air velocities.

Location	Δp (Pa)				
	1 m·s^{-1}	2 m·s^{-1}	3 m·s^{-1}	4 m·s^{-1}	5 m·s^{-1}
Upper	183.54	734.07	1651.60	2936.13	4587.65
Lateral	7.86	30.70	68.52	121.33	189.13

Table 2
Fitting equations and fitting goodness of ventilation panel pressure loss.

Location	Equation	R^2
Upper	$\Delta p = 183.5v^2 + 0.03622v$	1.000
Lateral	$\Delta p = 7.492v^2 + 0.3646v$	1.000

Table 3
Porous media parameters of the ventilation panel.

Location	C_2 (m^{-1})	$1/\alpha$ (m^{-2})
Upper	149 795	1 005 556
Lateral	3 058	5 063 889

In the numerical simulation, the porous media model of the ventilation panel was set using the porous cell zone condition in ANSYS Fluent, and the porous jump face model was set using the porous jump boundary condition. For the numerical simulation of the internal flow field of a subway car using these two models, the porous media parameters $1/\alpha$ and C_2 and the porosity rate are required. In the porous media model, the ventilation panel zone was defined as the "porous zone" in the "cell zone conditions" section. For the porous jump face model, the face of the ventilation panel was selected as the "porous jump" in the "boundary conditions" section, and the thickness of the ventilation panel, Δn, was entered.

4. Experimental verification and analysis

Three ventilation panel models were applied for comparison in this study. The numerical results were compared with data from a real-life experiment with the middle car of a subway train. The model that was able to effectively perform numerical simulation of the internal flow field of the subway car using the least computational power was then identified.

4.1. Real subway car experiment

An experiment using the middle car of a subway train was carried out at the Central South University model test platform in China. (Detailed information about the platform can be found in Refs. [30,31].) The real subway car used for the experiment had the dimensions shown in Fig. 1(a). Four XFH air conditioners from Yuete Ventilation Equipment Co. were selected, with each being able to produce a 2500 m^3·h^{-1} flow rate of 13 °C fresh air. There were four air inlets in the supply air duct, with one air conditioner corresponding to each. The fresh air produced from the air conditioners passed into the supply air duct directly. The recirculation and exhaust air ducts were not set up as a part of this experiment; instead, a ventilator was set at each recirculated and exhaust air outlet of the passenger compartment. The flow rates of each recirculation and exhaust ventilator were 3400 and 533 m^3·h^{-1}, respectively. A full-passenger working condition was simulated by the use of 310 heating coils, each with 120 W heating power. All the heating coils are uniformly placed on the floor of the passenger compartment. After the air conditioners and the heating coils had operated for about 30 min, the relevant flow field parameters in the passenger compartment were measured. At this time, the flow field structure and temperature in the passenger compartment can be expected to be stable, so these conditions could effectively simulate actual full-passenger working conditions in summer.

The pressure change in the passenger compartment was relatively small, and the pressure difference of the 1.1 m height horizontal plane (Z = 1.1 m) was less than 1 Pa. Thus, the pressure of the measurement points was not considered. The air velocity and temperature of the measurement points were obtained. The air velocity sensor was the same as that used in the ventilation panel model experiment. For temperature measurement, an AI5600 hand-held high-precision thermometer was adopted with a measurement accuracy of 0.01 °C. (The positions of the measurement points were given in Section 2.3.)

4.2. Experimental verification

Table 4 provides a comparison between the numerical simulation of the original model, porous media model, and porous jump face model with the experimental data obtained from the middle car of a subway train.

As can be observed from Table 4, the flow field parameters of the original model have the lowest numerical error, with each numerical error of the flow field parameter being less than 4%.

Table 4
Real subway car experiment data and numerical errors.

	Experimental data	Numerical errors		
		Original model	Porous media model	Porous jump face model
v_a	0.17 m·s^{-1}	3.19%	3.45%	10.59%
v_x	0.25 m·s^{-1}	−3.07%	−3.21%	8.40%
v_z	0.59 m·s^{-1}	−2.53%	−2.48%	−9.15%
T_a	26.90 °C	−3.98%	−4.71%	−4.13%
T_x	6.68 °C	−1.35%	1.65%	−5.39%
T_z	6.94 °C	1.30%	−1.87%	4.61%

The original model was built strictly based on the geometry of the ventilation panel. As a result, the numerical simulation result of the original model shows that the turbulence model and mesh selected in this study can effectively predict the internal flow field of a subway compartment. In other words, the simulation approach is validated by the experimental data.

The numerical simulation results of the porous jump face model in Table 4 differ significantly from the experimental data, and the numerical errors of some flow field parameters are over 8%. Therefore, the porous jump face model cannot be used for the numerical simulation of the internal flow field of a subway car. The flow field parameters of the porous media model have relatively small numerical errors, with a maximum numerical error of 4.71%, which meets the engineering requirements. The difference between the numerical results of the original model and those of the porous media model is less than 1%. Furthermore, in comparison with the original model, the porous media model provides a large reduction in computational power. Thus, in engineering applications, the porous media model could be used to replace the original model for the numerical simulation of the internal flow field of a subway car.

4.3. Internal flow field analysis

A comparison of the numerical simulation results of the porous media model with those of the original model can further illustrate the feasibility of replacing the original model with the porous media model.

In the real subway car experiment, 15 measurement points were chosen, based on the European standard EN14750, as shown in Fig. 5. These points were separated into two groups: a horizontal group and a vertical group. Each group corresponds to a plane. As a result, the 1.1 m height horizontal plane (Z = 1.1 m) and the symmetric vertical plane (Y = 0 m) were selected for the internal flow field analysis. Because of the combined effects of the supply, recirculated, and exhaust air system, the velocity field remained in a relatively stable state. The temperature outside the subway car was set at 33 °C and that of the fresh air was set at 13 °C. Taking into account the thermal energy produced by the human occupants of the car and the subway car's surface heat transfer, the temperature field inside the passenger compartment was maintained in a relatively balanced state. Thus, the velocity and temperature distributions of a typical section of the compartment could represent the velocity and temperature field inside the subway car. As the pressure change in the passenger compartment was relatively small, the pressure field was not studied.

Fig. 7 shows the velocity distributions of the original model and of the porous media model in two typical sections of the subway car at the same moment. As the turbulent flow is unsteady and the change range of the velocities of the two models is almost the same, the velocity fields of the two models are basically consistent. Due to the recirculated air system, the air velocity around the recirculated air outlets is greater than other part in the compartment. According to the definition in Section 2.3, the average velocity, horizontal velocity difference, and vertical velocity difference of the two models are basically consistent, which aligns with the results in Table 4.

Fig. 8 shows the temperature distributions of the original model and the porous media model of two typical sections of the subway car in the same moment. According to the figure, the temperature distributions of the two models of the passenger compartment basically agree, especially in the human-activity area. The upper half of End II is the highest temperature area in both models. The temperature is slightly higher in the upper half of End I than in the human-activity area. This temperature difference is caused by the location of the passenger compartment air inlet. As shown in Fig. 1, the air inlet of the passenger compartment is not distributed along the entire length of the subway car. The air inlets

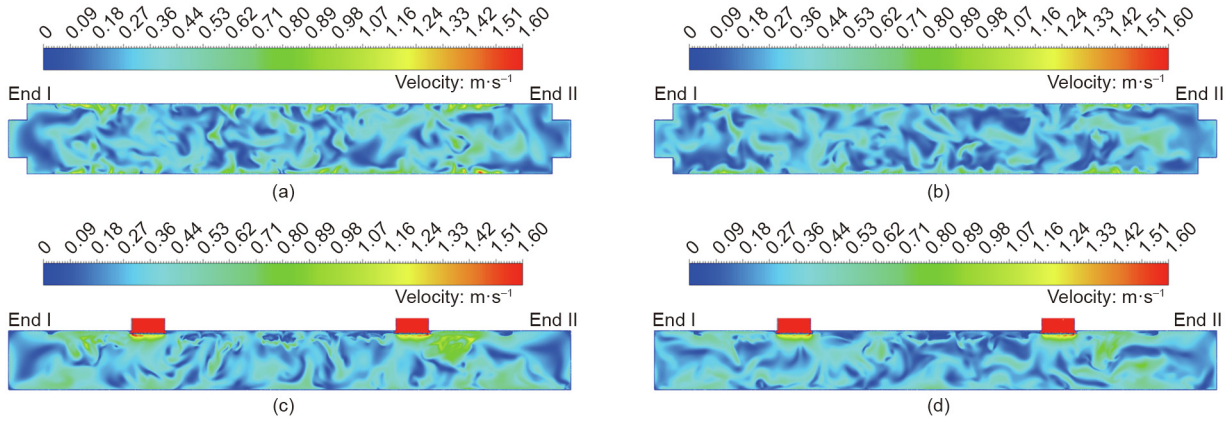

Fig. 7. Velocity distributions of typical sections of the subway car in the same moment. (a) Original model (Z = 1.1 m); (b) porous media model (Z = 1.1 m); (c) original model (Y = 0 m); (d) porous media model (Y = 0 m).

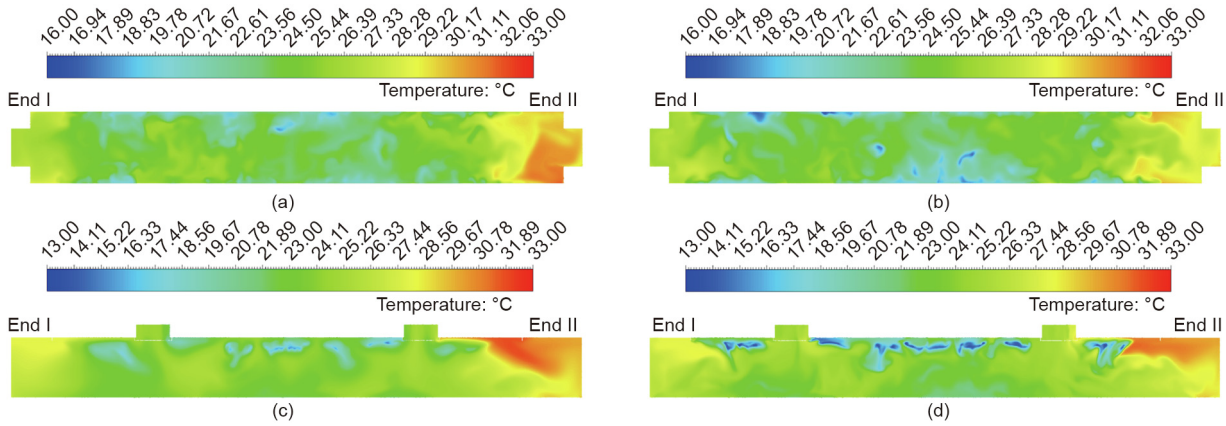

Fig. 8. The temperature distributions of typical sections of the subway car in the same moment. (a) Original model (Z = 1.1 m); (b) porous media model (Z = 1.1 m); (c) original model (Y = 0 m); (d) porous media model (Y = 0 m).

are not set at the front and back of the passenger compartment, and End II is farther away from the air inlet than End I. As the fresh air is cool, the temperature of End II is higher than that of End I, and the low-temperature zone is at the top of the compartment.

It can be observed from Figs. 8(a) and (b) that in the horizontal plane, the temperature of the original model is slightly higher than that of the porous media model at End II, although it is basically consistent in other zones. As a result, the average temperature of the original model is slightly higher than that of the porous media model, which is consistent with the results presented in Table 4. The temperature of the porous media model in some parts of the middle zone is lower than that of the original model, resulting in a greater horizontal temperature difference in the porous media model.

Figs. 8(c) and (d) show that in the vertical plane, the temperature of the original model is higher than that of the porous media model at End II. In the supply air inlet zone at the top of the passenger compartment, the minimum temperatures of the two models are basically consistent. As a result, the vertical temperature difference of the original model is slightly higher than that of the porous media model, as presented in Table 4.

Through this analysis of the velocity and temperature distributions of the typical sections, it can be concluded that the internal flow field distributions of the two models are in good agreement. Thus, the porous media model is a good alternative to the ventilation panel in the numerical simulation of the internal flow field of the subway car.

5. Conclusion

This work focused on the simplification of the numerical simulation model of ventilation panels in a subway passenger compartment. Two simplified numerical simulation models—the porous media model and the porous jump face model—were chosen and evaluated in order to improve the numerical calculation efficiency. The parameters required to define the porous media model and porous jump face model were determined by means of experimental data. The numerical simulation results of the two simplified models and the original model were compared with experimental data for a real subway car. The results showed that the porous media model could replace the original model in the flow field simulation of a subway passenger compartment, and provides a shorter computation time. The flow field parameters (temperature and velocity) of the porous media model had relatively small numerical errors, with a maximum numerical error among all parameters of 4.71%. The difference between the numerical results of the original model and those of the porous media model was less than 1%. The porous media model can reduce the computing resources by about 25%. Using the porous media model developed in this study, the air-supply uniformity in subway passenger compartments can be studied in a more effective manner.

Acknowledgements

The authors would like to thank Yuxiang Xi and Xin Liu for their contributions to the numerical simulation investigation. Tiantian Wang gratefully acknowledges financial support from the National Key R&D Program of China (2016YFB1200602-11 and 2016YFB1200602-12).

Compliance with ethics guidelines

Yu Tao, Mingzhi Yang, Bosen Qian, Fan Wu, and Tiantian Wang declare that they have no conflict of interest or financial conflicts to disclose.

References

[1] Chow WK. Ventilation of enclosed train compartments in Hong Kong. Appl Energy 2002;71(3):161–70.
[2] Dehghan MH, Abdolzadeh M. Comparison study on air flow and particle dispersion in a typical room with floor, skirt boarding, and radiator heating systems. Build Environ 2018;133:161–77.
[3] Zhuang R, Li X, Tu J. CFD study of the effects of furniture layout on indoor air quality under typical office ventilation schemes. Build Simul 2014;7(3):263–75.
[4] Pang L, Li P, Bai L, Liu D, Zhou Y, Yao J. Optimization of air distribution mode coupled interior design for civil aircraft cabin. Build Environ 2018;134:131–45.
[5] Zhang H, Dai L, Xu G, Li Y, Chen W, Tao W. Studies of air-flow and temperature fields inside a passenger compartment for improving thermal comfort and saving energy. Part I: test/numerical model and validation. Appl Therm Eng 2009;29(10):2022–7.
[6] Zhang H, Dai L, Xu G, Li Y, Chen W, Tao W. Studies of air-flow and temperature fields inside a passenger compartment for improving thermal comfort and saving energy. Part II: simulation results and discussion. Appl Therm Eng 2009;29(10):2028–36.
[7] Bianco V, Manca O, Nardini S, Roma M. Numerical investigation of transient thermal and fluidynamic fields in an executive aircraft cabin. Appl Therm Eng 2009;29(16):3418–25.
[8] Mao Y, Wang J, Li J. Experimental and numerical study of air flow and temperature variations in an electric vehicle cabin during cooling and heating. Appl Therm Eng 2018;137:356–67.
[9] Dullinger C, Struckl W, Kozek M. A modular thermal simulation tool for computing energy consumption of HVAC units in rail vehicles. Appl Therm Eng 2015;78:616–29.
[10] Hofstädter RN, Zero T, Dullinger C, Richter G, Kozek M. Heat capacity and heat transfer coefficient estimation for a dynamic thermal model of rail vehicles. Math Comput Model Dyn Syst 2017;23(5):439–52.

[11] Luger C, Kallinovsky J, Rieberer R. Identification of representative operating conditions of HVAC systems in passenger rail vehicles based on sampling virtual train trips. Adv Eng Inform 2016;30(2):157–67.
[12] Schmeling D, Bosbach J. On the influence of sensible heat release on displacement ventilation in a train compartment. Build Environ 2017;125:248–60.
[13] Li W, Sun J. Numerical simulation and analysis of transport air conditioning system integrated with passenger compartment. Appl Therm Eng 2013;50(1):37–45.
[14] Liu W, Deng Q, Huang W, Liu R. Variation in cooling load of a moving air-conditioned train compartment under the effects of ambient conditions and body thermal storage. Appl Therm Eng 2011;31(6–7):1150–62.
[15] Suárez C, Iranzo A, Salva JA, Tapia E, Barea G, Guerra J. Parametric investigation using computational fluid dynamics of the HVAC air distribution in a railway vehicle for representative weather and operating conditions. Energies 2017;10(8):1074–86.
[16] Wang H, Lin M, Chen Y. Performance evaluation of air distribution systems in three different China railway high-speed train cabins using numerical simulation. Build Simul 2014;7(6):629–38.
[17] Aliahmadipour M, Abdolzadeh M, Lari K. Air flow simulation of HVAC system in compartment of a passenger coach. Appl Therm Eng 2017;123:973–90.
[18] BS EN 14750-1: Railway applications—air conditioning for urban and suburban rolling stock. Part 1: comfort parameters. British standard. London: British Standards Institution; 2006.
[19] BS EN 14750-2: Railway applications—air conditioning for urban and suburban rolling stock. Part 2: type tests. British standard. London: British Standards Institution; 2006.
[20] Chen Z, Liu T, Zhou X, Niu JQ. Impact of ambient wind on aerodynamic performance when two trains intersect inside a tunnel. J Wind Eng Ind Aerodyn 2017;169:139–55.
[21] Niu J, Zhou D, Liang X, Liu T, Liu S. Numerical study on the aerodynamic pressure of a metro train running between two adjacent platforms. Tunn Undergr Space Technol 2017;65:187–99.
[22] Yan Y, Li X, Tu J. Effects of passenger thermal plume on the transport and distribution characteristics of airborne particles in an airliner cabin section. Sci Technol Built Environ 2016;22(2):153–63.
[23] Dehne T, Lange P, Volkmann A, Schmeling D, Konstantinov M, Bosbach J. Vertical ventilation concepts for future passenger cars. Build Environ 2018;129:142–53.
[24] Yang L, Li M, Li X, Tu J. The effects of diffuser type on thermal flow and contaminant transport in high-speed train (HST) cabins—a numerical study. Int J Vent 2018;17(1):48–62.
[25] Gray DD, Giorgini A. The validity of the Boussinesq approximation for liquids and gases. Int J Heat Mass Transf 1976;19(5):545–51.
[26] Bacharoudis E, Vrachopoulos MG, Koukou MK, Margaris D, Filios AE, Mavrommatis SA. Study of the natural convection phenomena inside a wall solar chimney with one wall adiabatic and one wall under a heat flux. Appl Therm Eng 2007;27(13):2266–75.
[27] Teitel M, Dvorkin D, Haim Y, Tanny J, Seginer I. Comparison of measured and simulated flow through screens: effects of screen inclination and porosity. Biosyst Eng 2009;104(3):404–16.
[28] Bejan A, Dincer I, Lorente S, Miguel AF, Reis AH. Porous and complex flow structures in modern technologies. New York: Springer; 2004.
[29] Fluent help. Pittsburgh: ANSYS Inc.; 2017.
[30] Yang M, Du J, Li Z, Huang S, Zhou D. Moving model test of high-speed train aerodynamic drag based on stagnation pressure measurements. PLoS ONE 2017;12(1):e0169471.
[31] Zhang L, Yang M, Liang X, Zhang J. Oblique tunnel portal effects on train and tunnel aerodynamics based on moving model tests. J Wind Eng Ind Aerodyn 2017;167:128–39.